*Published online 4 May 2011* *Nucleic Acids Research, 2011, Vol. 39, No. 15* ***6633–6645***
*doi:10.1093/nar/gkr274*

# Specific implications of the HIV-1 nucleocapsid zinc fingers in the annealing of the primer binding site complementary sequences during the obligatory plus strand transfer

**Julien Godet[1,2], Nick Ramalanjaona[1], Kamal K. Sharma[1], Ludovic Richert[1], Hugues de Rocquigny[1], Jean-Luc Darlix[3], Guy Duportail[1] and Yves Mély[1,*]**

[1]Laboratoire de Biophotonique et Pharmacologie, UMR 7213 CNRS, Université de Strasbourg, Faculté de Pharmacie, 74 route du Rhin, 67401 Illkirch, [2]Medical Information and Biostatistics Department, Strasbourg University Hospital, 67000 Strasbourg and [3]Unité de Virologie Humaine INSERM 758, IFR 128 Ecole Normale Supérieure de Lyon, 46 allée d'Italie, 69364 LYON, France

Received February 18, 2011; Revised and Accepted April 8, 2011

## ABSTRACT

**Synthesis of the HIV-1 viral DNA by reverse transcriptase involves two obligatory strand transfer reactions. The second strand transfer corresponds to the annealing of the (−) and (+) DNA copies of the primer binding site (PBS) sequence which is chaperoned by the nucleocapsid protein (NCp7). NCp7 modifies the (+)/(−)PBS annealing mechanism by activating a loop–loop kissing pathway that is negligible without NCp7. To characterize in depth the dynamics of the loop in the NCp7/PBS nucleoprotein complexes, we investigated the time-resolved fluorescence parameters of a (−)PBS derivative containing the fluorescent nucleoside analogue 2-aminopurine at positions 6, 8 or 10. The NCp7-directed switch of (+)/(−)PBS annealing towards the loop pathway was associated to a drastic restriction of the local DNA dynamics, indicating that NCp7 can 'freeze' PBS conformations competent for annealing via the loops. Moreover, the modifications of the PBS loop structure and dynamics that govern the annealing reaction were found strictly dependent on the integrity of the zinc finger hydrophobic platform. Our data suggest that the two NCp7 zinc fingers are required to ensure the specificity and fidelity of the second strand transfer, further underlining the pivotal role played by NCp7 to control the faithful synthesis of viral HIV-1 DNA.**

## INTRODUCTION

Human immunodeficiency virus type 1 (HIV-1) viral DNA synthesis is a complex multi-step process catalysed by the viral reverse transcriptase (RT). Synthesis of the complete viral DNA with long terminal repeats (LTR) requires two obligatory DNA transfer reactions. During the first strand transfer, the minus-strand strong-stop DNA [(−)ssDNA] is translocated to the 3′-end of the viral RNA genome through a reaction mediated by base pairing of the repeat sequences at the 3′-ends of the RNA and cDNA reactants, which in turn allows reverse transcription to resume and to continue up to the 5′-end of the primer binding site (PBS), (−) PBS. The second or plus strand transfer relies on (−)PBS annealing to the (+)PBS sequence located in the plus strand strong-stop DNA [(+)ssDNA] (1,2). The annealing of these two complementary PBS DNA stem–loops (Figure 1) enables RT to resume and complete viral DNA synthesis. These two obligatory strand transfers are chaperoned by the HIV-1 nucleocapsid protein (NCp7), a potent nucleic acid chaperone that plays major roles in the viral replication cycle (3–6). The mature NCp7 is a 55 amino acids protein encoded by the HIV-1 Gag polyprotein (Figure 1). It contains two highly conserved CCHC zinc fingers (ZFs) that coordinate zinc ions with high affinity (7). The two-folded ZFs are connected by a highly conserved basic sequence and flanked by N- and C-terminal basic domains. NCp7 binds PBS sequences with good affinity (8,9) and catalyses the annealing reactions of the complementary (+)/(−)PBS sequences (10,11) via its ability to

*To whom correspondence should be addressed. Tel: +33 (0)3 68 85 42 63; Fax: +33 (0)3 68 85 43 12; Email: yves.mely@unistra.fr

The authors wish it to be known that, in their opinion, the first two authors should be regarded as joint First Authors.

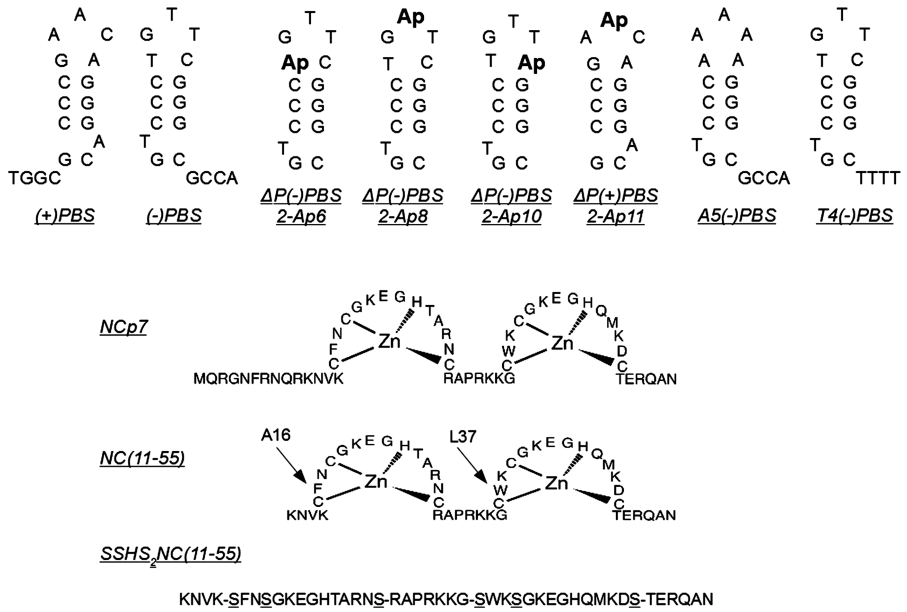


**Figure 1.** Sequences of the oligonucleotides and peptides used in this study.

chaperone the rearrangement of nucleic acids into their most thermodynamically stable conformations (6,12). In the absence of NCp7, (+)PBS can spontaneously anneal to (−)PBS *in vitro* (10). This annealing reaction proceeds mainly through the single-strand overhangs of the PBS sequences while nucleation through loop–loop interaction appears negligible (Figure 2). Interestingly, NCp7 was found to enhance the (−)/(+)PBS annealing kinetics by about 60-fold by strongly promoting the loop pathway, which thus becomes the major pathway (10). This switch in the annealing mechanism probably arises due to significant changes in the loop structure and/or dynamics of PBS upon NCp7 binding.

In agreement with this, structural changes of the loop were evidenced by solving the structure of NCp7 complexed to ΔP(−)PBS, a (−)PBS derivative without the 3′ protruding sequence (13). NCp7 was shown to preferentially bind to the 5′-end of the loop and the upper part of the stem. This binding is mediated by the hydrophobic plateau, involving the Val13, Phe16, Thr24, Ala25, Trp37, Gln45 and Met46 residues present on the top of the folded ZFs (14–16). The Phe16 and Trp37 residues insert between the T6 and G7 bases, allowing a tight stacking of the Trp37 residue with G7 (17), as well as the flipping of the T6 and G7 bases towards the exterior of the loop. Through this binding, NCp7 also stretches the loop, which increases the accessibility of the 8-TTC-10 nucleobases and slightly destabilizes the upper base pair (between 5-C and G-11) of the stem. A second binding site including the 10-CGG-12 segment was also identified but its structure with NCp7 could not be solved. As a consequence of the structural changes in PBS, NCp7 is thought to favour the PBS loop kissing interactions and help in disrupting their stem to convert the kissing complex into the final extended duplex.

To further characterize the molecular mechanism and protein determinants responsible for the (−)/(+)PBS annealing chaperoned by NCp7, we investigated the annealing mechanism by using PBS mutants and monitored the thermodynamic and kinetic parameters in presence of various NCp7 mutants. We also investigated the dynamic changes of both (−)PBS and (+)PBS loops in response to NCp7 binding by using PBS sequences labelled with 2-aminopurine (2-Ap), an environment-sensitive fluorescent analogue of adenine (18). We found that the integrity of ZFs was critical to modify the structure and restrict the dynamics of both PBS loops as well as to switch the annealing mechanism towards the loop–loop kissing

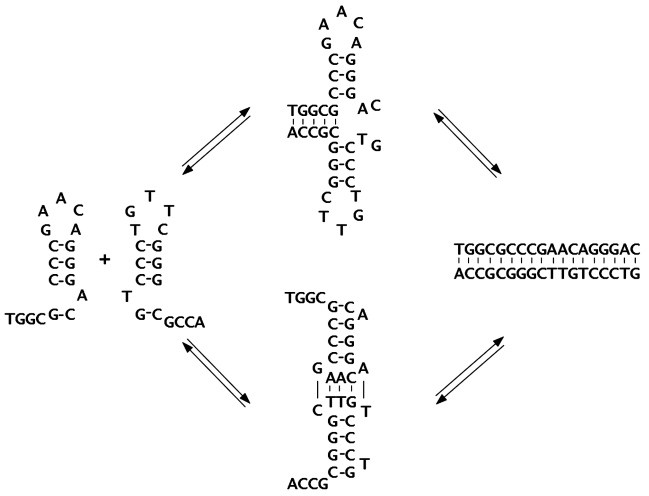


**Figure 2.** Mechanism for (−)/(+)PBS annealing as proposed by Ramalanjaona *et al.* (10). The (−)/(+)PBS annealing reaction can proceed through two major pathways. In these pathways, the final extended duplex can be nucleated either through the single-stranded overhangs (upper pathway) or through loop–loop interactions (lower pathway). In the absence of NCp7, the upper pathway is by far the most contributing one. NCp7 strongly activates the loop–loop kissing pathway, leading to a switch in the reaction mechanism.

pathway. The basic domains of NCp7 were able to modulate the annealing rate constants, but unable to modify the annealing mechanism. Thus, our data indicated that the hydrophobic plateau at the top of the folded ZFs is needed to direct the formation of competent PBS loop conformations for the annealing reaction, which ensures the specificity of the second strand transfer reaction.

## MATERIALS AND METHODS

### Materials

The NCp7, NC(11–55), $(SSHS)_2$NC(11–55), $L_{37}$NC(11–55) and $A_{16}$NC(11–55) peptides were synthesized on a Applied Biosystems A433 peptide synthesizer, as described (19,20). Unmodified or labelled oligonucleotides (ODNs) were synthesized and HPLC- or PAGE-purified by IBA Gmbh Nucleic Acids Product Supply (Germany). A 2′-deoxyribosyl-2-aminopurine (2-Ap) was selectively introduced at different positions (6, 7 or 10) within the ΔP(−)PBS loop and at position 11 of ΔP(+)PBS, substituting the corresponding natural base. Doubly labelled (+)PBS sequences were modified at their 5′ terminus with 6-carboxyrhodamine (Rh6G) and their 3′-terminus with 4-(4′-dimethylaminophenylazo)benzoic acid (DABCYL), via an amino linker with a six carbon spacer arm. All experiments were performed in 25 mM TRIS–HCl, pH 7.5, 30 mM NaCl and 0.2 mM $MgCl_2$ at 20°C, unless specified otherwise.

### Steady-state fluorescence spectroscopy

Fluorescence emission spectra were recorded with a Fluorolog or a Fluoromax-3 spectrofluorimeter (Jobin Yvon) equipped with a thermostated cell compartment. All fluorescence intensities were corrected for screening effects, buffer emission and lamp fluctuations. The quantum yield was calculated using free 2-Ap riboside as a reference [quantum yield = 0.68 (18)]. 2-Ap was excited at 315 nm.

Kinetics of (−)/(+)PBS annealing was monitored in real-time using fluorescent doubly labelled (+)PBS sequences and non-labelled (−)PBS. Excitation and emission wavelengths were at 520 nm and 550 nm, respectively, to monitor the fluorescence restoration of Rh6G resulting from the formation of the (−)/(+)PBS duplex. Concentrations of 5′Rh6G-(+)PBS-3′DABCYL and (−)PBS were 10 nM and 100 nM to 1.1 μM, respectively, to ensure pseudo-first order conditions. Both reactants (in identical volumes) coated by NC peptides were mixed together to trigger the reaction. The apparent rate constants $k_{obs}$ were determined from the kinetic data, as previously described (10). All fitting procedures were carried out with the Microcal Origin 6.1 software based on non-linear least-squares methods, applying the Levenberg-Marquardt algorithm.

### Time-resolved fluorescence measurements

Time-resolved fluorescence measurements were performed with the time correlated, single-photon counting technique. Excitation pulses were generated by a pulse-picked frequency-tripled Ti-sapphire laser (Tsunami, Spectra Physics) pumped by a Millenia X laser (Spectra Physics) (21). Excitation wavelength was set at 315 nm, with a repetition rate of 4 MHz. The fluorescence emission was collected through a polarizer set at magic angle and a 16 mm band-pass monochromator (Jobin Yvon) at 370 nm. The single-photon events were detected with a micro-channel plate photomultiplier (Hamamatsu) either coupled to a pulse pre-amplifier (Philips) and recorded on a multi-channel analyser (Ortec) calibrated at 25.5 ps/channel or coupled to a pulse pre-amplifier HFAC (Becker-Hickl) and recorded on a SPC-130 board (Becker-Hickl). The instrumental response function (IRF) was recorded using a polished aluminium reflector, and its full-width at half-maximum was ∼40 ps. The mean lifetime $\langle\tau\rangle$ was calculated from the individual fluorescence lifetimes ($\tau_i$) and their relative amplitudes ($\alpha_i$) according to $\langle\tau\rangle = \Sigma\alpha_i\tau_i$. The population, $\alpha_0$, of dark species of 2-Ap was calculated by: $\alpha_0 = 1-\tau_{free}/(\tau_{ODN} \times R_m)$, where $\tau_{free}$ is the lifetime of the free 2-Ap, $\tau_{ODN}$ is the measured mean lifetime of 2-Ap within the ODN and $R_m$ is the ratio of their corresponding quantum yields. The remaining amplitudes, $\alpha_{ic}$ were recalculated from the measured amplitudes according to $\alpha_{ic} = \alpha_i \times (1-\alpha_0)$.

Time-resolved anisotropy, resulting from the measurement of the fluorescence decay curves recorded in directions parallel ($I_{//}$) and perpendicular ($I_\perp$) alternatively, to the excitation beam polarization, was analysed by the following equations:

$$I_{//}(t) = \frac{I(t)[1+2r(t)]}{3} \quad (1)$$

$$I_\perp(t) = \frac{I(t)[1-2r(t)]}{3} \quad (2)$$

$$r(t) = \frac{I_{//}(t) - G \times I_\perp(t)}{I_{//}(t)+2G \times I_\perp(t)} = r_0 \sum_i \beta_i \times \exp\left(-\frac{t}{\Phi_i}\right) \quad (3)$$

where $\beta_i$ are the amplitudes of the rotational correlation times $\Phi_i$, and $G$ is the geometry factor at the emission wavelength, determined in independent experiments. Theoretical values of the rotational correlation times and the values of the cone semi-angle $\theta_0$ of the local motion of 2-Ap were calculated as described in the Supplementary Data. Time-resolved intensity and anisotropy data were treated according to the maximum entropy method (Pulse 5 software) (22,23) or according to a non-linear least-square analysis using a homemade software (kindly provided by G. Krishnamoorthy). In all cases, the $\chi^2$ values were close to 1 and the weighted residuals as well as their autocorrelation were distributed randomly around 0, indicating an optimal fit.

## RESULTS

### Characterization of the ΔP(−)PBS and ΔP(+)PBS sequences labelled with 2-Ap

In the ΔP(−)PBS, 2-Ap was introduced either within (2-Ap6) or adjacent to (2-AP8) to the critical 5-CTG-7 segment of the major binding site for NCp7 at the 5′

end of the loop, or within the low affinity binding site (2-Ap10) at the 3′ end of the loop (Figure 1). Since 2-Ap is able to locally report on the dynamics of the ODN sequence in which it is inserted, these three substitutions were aimed to site-specifically probe the two binding sites. The quantum yield of the 2-Ap residues inserted in ΔP(−)PBS was largely reduced as compared to the free probe (18) (Table 1), indicating a strong fluorescence quenching by its neighbouring bases (24). The quenching was the most pronounced for 2-Ap at position 10, suggesting a strong stacking with G11. This inferred stacking is in full line with the stacking of C10 with G11 according to NMR analyses (13), indicating that substitution of C10 by 2-Ap likely preserves the local structure of the loop. Taking into account that each 2-Ap was flanked by a guanine, the most efficient quencher of 2-Ap among the natural bases (25), the quantum yield of 2-Ap at positions 6 and 8 appeared comparatively higher than the quantum yields observed in single-stranded ODNs (26–28). This suggested that the PBS loop is at least partially ordered, so that efficient collisions of the 2-Ap with its neighbour bases, and notably with the G7 base, are lowered. This is again in line with the NMR data (13) since the T8 base was found to be perpendicular to the G7 residue, while the T6 base could stack with C5 but not with G7. Thus, our data strongly suggest that substitutions of the natural bases by 2-Ap only marginally perturb the native folding of the loop.

The time-resolved intensity decays of the 2-Ap-labelled ODNs were complex, showing that conformational fluctuations of the loop occurred during the excited state of the 2-Ap residues. These decays were best fitted with four discrete lifetime components, ranging from 0.1 ns to nearly 9 ns (Table 1), indicating that 2-Ap experienced at least four conformational states. Moreover, additional conformations associated to ultra-short-lived lifetimes below the time resolution of our set-up have to be considered (27), as a striking difference between the mean lifetimes of 2-Ap labelled ODNs and their corresponding quantum yields was observed. Indeed, the mean lifetimes were found to be only 4–6.5 times shorter than the 10.2 ns lifetime of the free 2-Ap, while their quantum yields differed by factors 25–155. These dark-species were previously shown to result from ultra-fast dynamic quenching (29).

Dark-species and weakly emitting species were by far the most populated conformations since they represented ~90% of the 2-Ap conformations, as it could be seen from the sum of the $\alpha_0$ and $\alpha_1$ amplitudes (Table 1). This efficient dynamic quenching of 2-Ap by its neighbour residues can be related to conformational fluctuations of the loop in the picosecond–nanosecond (ps–ns) range, allowing quenching of 2-Ap through a charge transfer mechanism (29–32). The stacked conformations arose to 98% for 2-Ap10, further confirming a strong stacking with G11. The values of the longer lived lifetime $\tau_4$, associated to extra-helical or unstacked conformations, were close to the lifetime of free 2-Ap, but low populated, representing from 1% to 4% of the whole conformations (Table 1). The high value of the long-lived $\tau_4$ lifetime confirmed the limited flexibility of the (−)PBS loop, since in short

**Table 1.** Steady-state and time-resolved fluorescence parameters of 2-Ap-substituted ΔP(–)PBS and ΔP(+)PBS

| | Quantum yield | $\alpha_0$ | $\tau_1$ | $\alpha_1$ | $\tau_2$ | $\alpha_2$ | $\tau_3$ | $\alpha_3$ | $\tau_4$ | $\alpha_4$ | $\langle\tau\rangle$ |
|---|---|---|---|---|---|---|---|---|---|---|---|
| Free 2-Ap riboside | 0.680[a] | – | – | – | – | – | – | – | 10.2 | 1.00 | 10.2 |
| ΔP (−)PBS 2-Ap6 | 0.024 | 0.80 | 0.10 | 0.13 | 0.7 | 0.02 | 3.6 | 0.02 | 8.0 | 0.03 | 1.8 |
| ΔP (−)PBS 2-Ap6 + NCp7 | 0.044 | 0.72 | 0.12 | 0.10 | 0.6 | 0.07 | 2.8 | 0.06 | 8.3 | 0.05 | 2.4 |
| ΔP (−)PBS 2-Ap6 + NC(11–55) | 0.040 | 0.75 | 0.12 | 0.10 | 0.6 | 0.06 | 3.4 | 0.04 | 7.5 | 0.05 | 2.3 |
| ΔP (−)PBS 2-Ap6 + $SSHS_2$NC(11–55) | 0.024 | 0.80 | 0.09 | 0.08 | 0.6 | 0.04 | 2.9 | 0.06 | 7.5 | 0.02 | 2.0 |
| ΔP (−)PBS 2-Ap6 + $A_{16}$NC(11–55) | 0.026 | 0.78 | 0.11 | 0.11 | 0.7 | 0.04 | 3.1 | 0.04 | 8.3 | 0.03 | 1.8 |
| ΔP (−)PBS 2-Ap6 + $L_{37}$NC(11–55) | 0.035 | 0.62 | 0.10 | 0.20 | 0.7 | 0.07 | 3.3 | 0.06 | 8.7 | 0.05 | 1.9 |
| ΔP (−)PBS 2-Ap8 | 0.028 | 0.82 | 0.09 | 0.08 | 0.7 | 0.03 | 3.1 | 0.03 | 8.3 | 0.04 | 2.1 |
| ΔP (−)PBS 2-Ap8 + NCp7 | 0.087 | 0.60 | 0.09 | 0.13 | 0.6 | 0.08 | 3.8 | 0.08 | 8.9 | 0.11 | 3.3 |
| ΔP (−)PBS 2-Ap8 + NC(11–55) | 0.081 | 0.60 | 0.14 | 0.13 | 0.6 | 0.10 | 3.8 | 0.07 | 8.5 | 0.10 | 3.0 |
| ΔP (−)PBS 2-Ap8 + $SSHS_2$NC(11–55) | 0.032 | 0.80 | 0.10 | 0.09 | 0.7 | 0.04 | 3.2 | 0.04 | 8.2 | 0.03 | 2.1 |
| ΔP (−)PBS 2-Ap8 + $A_{16}$NC(11–55) | 0.033 | 0.70 | 0.07 | 0.17 | 0.7 | 0.05 | 3.2 | 0.04 | 8.2 | 0.04 | 2.0 |
| ΔP (−)PBS 2-Ap8 + $L_{37}$NC(11–55) | 0.035 | 0.79 | 0.10 | 0.09 | 0.9 | 0.04 | 3.6 | 0.04 | 8.9 | 0.04 | 2.5 |
| ΔP (−)PBS 2-Ap10 | 0.006 | 0.94 | 0.13 | 0.03 | 0.8 | 0.01 | 3.5 | 0.01 | 8.2 | 0.01 | 2.1 |
| ΔP (−)PBS 2-Ap10 + NCp7 | 0.028 | 0.83 | 0.13 | 0.08 | 0.7 | 0.03 | 4.3 | 0.04 | 8.8 | 0.02 | 2.7 |
| ΔP (−)PBS 2-Ap10 + NC(11–55) | 0.021 | 0.86 | 0.15 | 0.07 | 0.7 | 0.03 | 3.9 | 0.02 | 8.6 | 0.02 | 2.3 |
| ΔP (−)PBS 2-Ap10 + $SSHS_2$NC(11–55) | 0.007 | 0.92 | 0.10 | 0.03 | 0.8 | 0.02 | 3.9 | 0.02 | 8.3 | 0.01 | 2.0 |
| ΔP (−)PBS 2-Ap10 + $A_{16}$NC(11–55) | 0.008 | 0.95 | 0.07 | 0.02 | 0.6 | 0.01 | 2.9 | 0.01 | 7.5 | 0.01 | 2.1 |
| ΔP (−)PBS 2-Ap10 + $L_{37}$NC(11–55) | 0.009 | 0.95 | 0.09 | 0.02 | 0.8 | 0.01 | 3.1 | 0.01 | 8.2 | 0.01 | 2.6 |
| ΔP (+)PBS 2-Ap11 | 0.036 | 0.50 | 0.09 | 0.34 | 0.8 | 0.09 | 3.6 | 0.03 | 8.2 | 0.04 | 1.1 |
| ΔP (+)PBS 2-Ap11 + NCp7 | 0.064 | 0.51 | 0.10 | 0.21 | 0.9 | 0.11 | 3.4 | 0.06 | 8.9 | 0.11 | 2.6 |
| ΔP (+)PBS 2-Ap11 + NC(11–55) | 0.061 | 0.51 | 0.10 | 0.22 | 0.7 | 0.12 | 3.6 | 0.07 | 8.8 | 0.08 | 2.1 |
| ΔP (+)PBS 2-Ap11 + $SSHS_2$NC(11–55) | 0.036 | 0.52 | 0.10 | 0.29 | 0.9 | 0.11 | 3.5 | 0.05 | 8.4 | 0.03 | 1.1 |

[a]Data from Ward *et al.* (18).

$\tau_i$ (ns) are the fluorescence lifetimes, $\alpha_i$ their amplitudes. The amplitude $\alpha_0$ of the dark species, as well as the amplitudes of the various lifetimes were calculated as described in the 'Materials and Methods' section. $\langle\tau\rangle$ is the mean fluorescence lifetime. SDs for the lifetimes and amplitudes are <15%.

ss-DNAs the corresponding lifetime did not exceed 5 ns (27,33), due to efficient collisions caused by the high flexibility of these sequences during the probe lifetime. Moreover, the low amplitude $\alpha_4$ observed for 2-Ap6, 2-Ap8 and 2-Ap10, suggested marginal exposure of bases towards the solvent, in full agreement with the orientation of the bases towards the interior of the PBS loop (13,34).

The local dynamics of the 2-Ap residues was further explored by time-resolved fluorescence anisotropy, which provides information on their rotational dynamics. Fluorescence anisotropy decays were adequately fitted with a three-exponential model (Table 2 and Figure 3). The two shorter components presumably correspond to the local rotation of the dye and the segmental mobility of the loop, respectively. The slowest correlation time of 2.1–2.6 ns was attributed to the global tumbling of the DNA sequence. Its deviation from the theoretical correlation time (1.75 ns) calculated for a sphere with the same molecular mass than the ODN (35) was related to the non-spherical shape of the PBS stem–loop. The relative amplitude of the fastest component allowed the estimation of the angular range for the local motion of 2-Ap, defined by the semi-angle cone ($\theta_0$) model (see Supplementary Data). These angles were found similar for the 2-Ap residues at the three positions and significantly lower to those observed in small single-stranded ODNs (26–28), confirming that the degree of freedom of the ΔP(−)PBS loop bases was restricted as compared to ssDNAs. The restricted rotation of the 2-Ap bases is in line with the internal orientation of the corresponding bases in the loop, which provides a relatively crowded environment (13,34).

To determine whether the dynamics of the (+)PBS loop was similar to that of (−)PBS, we site-specifically modified ΔP(+)PBS at position 11 with 2-Ap (Figure 1). The quantum yield of 2-Ap11 in ΔP(+)PBS was somewhat higher than in the ΔP(−)PBS derivatives, as a result of a

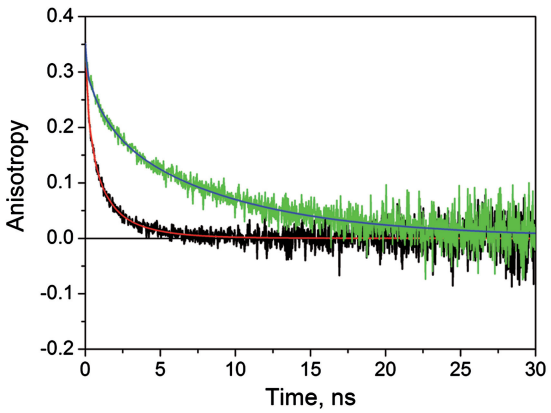


**Figure 3.** Experimental anisotropy decay curve of ΔP(−)PBS 2-Ap6 in the absence (black) and in the presence of NCp7 (green). The continuous lines (red and blue) correspond to the fit of the data with the parameters in Table 2.

**Table 2.** Fluorescence anisotropy decay parameters of 2-Ap-substituted ΔP(−)PBS and ΔP(+)PBS

| | $\Phi_1$ | $\beta_1$ | $\Phi_2$ | $\beta_2$ | $\Phi_3$ | $\beta_3$ | S | $\theta_0$ |
|---|---|---|---|---|---|---|---|---|
| Free 2-Ap riboside | 0.08 | 1.00 | – | – | – | – | 0.00 | 90 |
| ΔP (−)PBS 2-Ap6 | 0.17 | 0.38 | 0.7 | 0.34 | 2.2 | 0.28 | 0.79 | 32 |
| ΔP (−)PBS 2-Ap6 + NCp7 | 0.20 | 0.15 | 1.5 | 0.22 | 9.7 | 0.63 | 0.88 | 19 |
| ΔP (−)PBS 2-Ap6 + NC(11–55) | 0.17 | 0.18 | 1.2 | 0.28 | 7.4 | 0.54 | 0.91 | 21 |
| ΔP (−)PBS 2-Ap6 + $SSHS_2$NC(11–55) | 0.18 | 0.32 | 1.2 | 0.21 | 9.5 | 0.47 | 0.82 | 29 |
| ΔP (−)PBS 2-Ap6 + $A^{16}$NC(11–55) | 0.08 | 0.28 | 1.2 | 0.31 | 9.4 | 0.41 | 0.85 | 27 |
| ΔP (−)PBS 2-Ap6 + $L^{37}$NC(11–55) | 0.14 | 0.21 | 1.2 | 0.33 | 9.0 | 0.46 | 0.89 | 23 |
| ΔP (−)PBS 2-Ap8 | 0.22 | 0.36 | 0.7 | 0.11 | 2.1 | 0.53 | 0.79 | 31 |
| ΔP (−)PBS 2-Ap8 + NCp7 | 0.13 | 0.13 | 1.3 | 0.25 | 10.2 | 0.62 | 0.91 | 17 |
| ΔP (−)PBS 2-Ap8 + NC(11–55) | 0.13 | 0.13 | 0.9 | 0.32 | 7.7 | 0.55 | 0.93 | 17 |
| ΔP (−)PBS 2-Ap8 + $SSHS_2$NC(11–55) | 0.18 | 0.30 | 1.1 | 0.27 | 9.3 | 0.43 | 0.84 | 28 |
| ΔP (−)PBS 2-Ap8 + $A^{16}$NC(11–55) | 0.10 | 0.18 | 0.6 | 0.24 | 7.8 | 0.58 | 0.87 | 21 |
| ΔP (−)PBS 2-Ap8 + $L^{37}$NC(11–55) | 0.20 | 0.26 | 1.2 | 0.24 | 9.1 | 0.50 | 0.83 | 25 |
| ΔP (−)PBS 2-Ap10 | 0.18 | 0.46 | 0.9 | 0.27 | 2.6 | 0.27 | 0.73 | 36 |
| ΔP (−)PBS 2-Ap10 + NCp7 | 0.22 | 0.16 | 0.8 | 0.24 | 9.2 | 0.60 | 0.91 | 19 |
| ΔP (−)PBS 2-Ap10 + NC(11–55) | 0.20 | 0.21 | 0.9 | 0.20 | 7.5 | 0.59 | 0.89 | 23 |
| ΔP (−)PBS 2-Ap10 + $SSHS_2$NC(11–55) | 0.16 | 0.38 | 0.9 | 0.20 | 9.1 | 0.42 | 0.79 | 32 |
| ΔP (−)PBS 2-Ap10 + $A^{16}$NC(11–55) | 0.10 | 0.36 | 0.8 | 0.24 | 7.3 | 0.40 | 0.80 | 31 |
| ΔP (−)PBS 2-Ap10 + $L^{37}$NC(11–55) | 0.15 | 0.32 | 1.2 | 0.33 | 9.1 | 0.35 | 0.82 | 29 |
| ΔP (+)PBS 2-Ap11 | 0.12 | 0.32 | 0.6 | 0.21 | 2.2 | 0.47 | 0.82 | 29 |
| ΔP (+)PBS 2-Ap11 + NCp7 | 0.13 | 0.22 | 0.8 | 0.19 | 8.2 | 0.59 | 0.88 | 23 |
| ΔP (+)PBS 2-Ap11 + NC(11–55) | 0.10 | 0.25 | 0.9 | 0.20 | 7.8 | 0.55 | 0.89 | 25 |
| ΔP (+)PBS 2-Ap11 + $SSHS_2$NC(11–55) | 0.15 | 0.30 | 0.9 | 0.18 | 8.3 | 0.52 | 0.89 | 28 |

$\Phi_i$ (ns) are the rotational correlation times, $\beta_i$ their amplitudes, $S$ is the generalized order parameter and $\theta_0$ the cone semi-angle (in °) for 2-Ap local motion (calculated as described in the Supplementary Data). SDs for the rotational correlation times and amplitudes are <20% and <15%, respectively. The fluorescence anisotropy decay parameters are obtained from the fits of the time-resolved anisotropy decays, as illustrated in Figure 2.

sharp decrease of the $\alpha_0$ value in favour of the amplitudes associated to the $\tau_1$ and $\tau_2$ lifetimes, likely due to the absence of guanine residues flanking the 2-Ap11 residue (26,27). As for the ΔP(−)PBS derivatives, the number of lifetimes and distribution of amplitudes for 2-Ap11 in ΔP(+)PBS were in line with fast conformational fluctuations in the ps–ns range. Moreover, the $\tau_4$ and $\alpha_4$ values, as well as the time-resolved fluorescence anisotropy parameters, were very similar to those in ΔP(−)PBS, also leading to the conclusion of a partial order within the loop of ΔP(+)PBS. Taken together, our data suggest that the dynamics of the ΔP(+)PBS loop is similar to that of ΔP(−)PBS.

### Effect of NCp7 on the dynamics of the ΔP(−)PBS and ΔP(+)PBS loop

To characterize the effect of NCp7 on the dynamics of the ΔP(−)PBS and ΔP(+)PBS loops through the 2-Ap fluorescence changes, we first checked the impact of the 2-Ap substitutions on the binding of NCp7 to these PBS derivatives. By monitoring the binding of the 2-Ap-labelled ODNs to NCp7 through the quenching of the intrinsic Trp37 residue (36,37), we found that the 2-Ap substitutions did not induce significant changes in the binding parameters (see Supplementary Data), again in line with the aforementioned marginal changes induced by 2-Ap substitutions in the PBS structure.

Binding of NCp7 to the 2-Ap-labelled ODNs at a ratio of 3:1, to ensure saturation of the two protein binding sites on the loop (13), did not modify the maximum fluorescence emission wavelength of 2-Ap, but increased 2- to 5-fold its quantum yield (Table 1). As a consequence, the binding of NCp7 on ΔP(−)PBS or ΔP(+)PBS loop significantly reduced the level of quenching of 2-Ap fluorescence by its neighbouring bases but did not change the polarity of its environment. Furthermore, the time-resolved intensity decays revealed that the increase in the 2-Ap quantum yield was mainly due to decreased populations of the dark species benefiting the most emitting species, as well as to an increase in the long-lived $\tau_4$ lifetime value. These changes in the amplitude and lifetime values suggested that NCp7 severely restricted the stacking and collisions of 2-Ap with its neighbour residues. This restriction in stacking and collisions is in line with the ability of NCp7 to stretch the entire ΔP(−)PBS loop and to direct the T6 and G7 bases toward the exterior of the loop (13), which markedly increases the distance between the bases. In this respect, the large changes in the amplitudes and $\tau_4$ values observed for 2-Ap at position 8 of ΔP(−)PBS, are likely a consequence of the stacking of the Trp37 residue with G7, which prevents its collisions and stacking with 2-Ap8. Furthermore, the large changes in the amplitudes and $\tau_4$ values of 2-Ap10 at the 3′-end of the ΔP(−)PBS loop indicate that the binding of NCp7 to its second site in the loop induces similar restrictions on the stacking and collisions of 2-Ap.

Time-resolved anisotropy decays further revealed that binding of NCp7 to the ΔP(−)PBS loop induced a strong decrease in the amplitude associated with the local motion of the 2-Ap bases, irrespective of their position in the loop. The restriction of the local motion of the bases at positions 6 and 8, is fully consistent with numerous contacts between NCp7 and these bases, as observed by NMR upon binding to the loop 5′-end (13). Interestingly, we observed that binding of NCp7 to the 3′-end of the loop induced a similar freezing of the local motion of 2-Ap at position 10, suggesting that NCp7 induced similar restrictions on the local mobility of the bases in its two binding sites. The binding of at least two NCp7 molecules on the 2-Ap-labelled ODNs was clearly confirmed by the 9–10 ns value of the slowest correlation time $\Phi_3$, which is in line with the expected theoretical value of a 2:1 non-spherical complex. Interestingly, in all ΔP(−)PBS derivatives, the amplitude associated with the $\Phi_3$ correlation time strongly increased upon binding with NCp7, showing an overall decrease in the loop flexibility, so that the stem–loop tumbles as a whole. Taken together, our data indicate that NCp7 binding to its two binding sites on ΔP(−)PBS loop strongly restricts the picosecond to nanosecond dynamics of the loop, by constraining both the overall flexibility of the loop and the local mobility of the bases. The restricted dynamics of the loop majorly results in unstacking of bases. Similar conclusions can be drawn from the time-resolved anisotropy decays of ΔP(+)PBS, suggesting that NCp7 constrains both the overall and local dynamics of the two DNA PBS loops.

### Effect of NCp7 mutants on the dynamics of the ΔP(−)PBS and ΔP(+)PBS loop

To identify the protein determinants responsible for the NCp7-induced changes in the structure and dynamics of the ΔP(−)PBS and ΔP(+)PBS loops, we used a series of NCp7 mutants (Figure 1). The contribution of the N-terminal domain was investigated with NC(11–55), a peptide composed of the ZF domain but lacking the basic N-terminal domain. Binding of NC(11–55) to ΔP(−)PBS labelled by 2-Ap at positions 6, 8 or 10 or to ΔP(+)PBS labelled at position 11 induced changes in both steady-state and time-resolved fluorescence parameters similar to those of NCp7 (Tables 1 and 2), indicating that the NCp7-induced modifications in the structure and dynamics of the ΔP(−)PBS or ΔP(+)PBS loop are mainly mediated by the ZF domain.

Since NC(11–55) represented the minimal sequence able to constrain the PBS loop structure and dynamics in a manner very similar to NCp7, we studied the impact of mutants derived from this minimal NC sequence. We first investigated the role of the $Zn^{2+}$-induced folding of the NCp7 fingers, by using the $(SSHS)_2$NC(11–55) mutant where all cysteins are substituted by serines, in order to prevent the binding of zinc and subsequently the folding of the fingers (38,39). Binding of this mutated peptide to the 2-Ap-labelled ODNs was evidenced by the large increase of the $\Phi_3$ correlation time (Table 2), suggesting that at least two peptides did bind to the ODN. However, in sharp contrast to NCp7 and NC(11–55), $(SSHS)_2$NC(11–55) induced negligible changes in the steady-state and time-resolved parameters of the 2-Ap-labelled ODNs, indicating that this mutant only slightly restricts the flexibility of the loops and the local mobility of the bases.

Thus, the folding of the ZFs appears critical for the NCp7-induced changes in the structure and dynamics of the ΔP(−)PBS and ΔP(+)PBS loop.

Next, the contribution of the hydrophobic plateau at the top of the two ZFs was investigated by mutating the two conserved aromatic residues of this plateau that play a critical role in ODN binding (40–42). To that end, $Phe_{16}$ and $Trp_{37}$ were substituted by Ala and Leu in the $A_{16}$NC(11–55) and $L_{37}$NC(11–55) mutants, respectively. Since these two amino acids are not involved in zinc chelation, these mutations were expected to sustain the folding of the ZFs (15). Due to their limited affinity for ODNs (27), $A_{16}$NC(11–55) and $L_{37}$NC(11–55) peptides were added in large excess (1 peptide per 2 nt and 1 peptide to 1 nt, respectively), to ensure full coating of ΔP(−)PBS, as evidenced by the large $\Phi_3$ values similar to values obtained with NC(11–55). Both $A_{16}$NC(11–55) and $L_{37}$NC(11–55) mutants induced only a limited increase in the quantum yield of the different 2-Ap-substituted ΔP(−)PBS sequences, suggesting that these mutations dramatically alter the ability of NCp7 to reduce base stacking and restrict base collisions. This was confirmed by the limited lifetime redistribution towards the less quenched conformations. In addition, the two mutants moderately restricted the local mobility of 2-Ap as compared to NC(11–55), indicating the critical role played by the hydrophobic platform in this process. Moreover, it should be noted that these two mutants showed asymmetric effects with respect to the unstacking of 2-Ap at positions 6 and 8. Indeed, $A_{16}$NC(11–55) was more efficient than $L_{37}$NC(11–55) in reducing the amplitude $\alpha_0$ associated to dark species (0.70 versus 0.79) and the local mobility of 2-Ap in position 8 ($\beta_1 = 0.18$ versus 0.26). In contrast, at position 6, $L_{37}$NC(11–55) appeared more efficient ($\alpha_0 = 0.62$ versus 0.78 and $\beta_1 = 0.21$ verus 0.28). This asymmetric effect was consistent with NMR data showing that in the NC(12–53)/ΔP(−)PBS complex, $F_{16}$ interacts with T6 while $W_{37}$ interacts with G7(13).

These observations indicate that the ability of NCp7 to unstack and reorient the bases of the loop as well as to restrict the local and overall dynamics of ΔP(−)PBS or ΔP(+)PBS is mainly mediated by the hydrophobic plateau at the top of the ZFs.

### NCp7-mediated restriction of the PBS loop dynamics in the (−)/(+)PBS annealing reaction

To further evaluate the relevance of the NCp7-induced restriction of the dynamics of PBS loop, and notably its contribution to the promotion of (−)/(+)PBS annealing, we studied the annealing reaction of doubly labelled (+)PBS with non-labelled (−)PBS in the presence of NCp7 and NC mutants. The initial fluorescence of the folded 5′Rh6G-(+)PBS-3′DABCYL was very low due to its stem–loop structure, that brings the Rh6G fluorophore in close vicinity to the DABCYL group, acting as a quencher. Addition of NCp7 or NC(11–55) to the doubly labelled (+)PBS at a ratio of one NCp7 per 5 nt induced a small fluorescence increase, in line with the weak destabilizing activity of NCp7 on the PBS stem (9). In contrast, the $(SSHS)_2$NC(11–55) or $L_{37}$NC(11–55) mutants did not induce any increase in the Rh6G fluorescence, confirming the critical role of Trp37 residue and ZFs in NCp7 destabilizing activity (40). Addition of (−)PBS to 5′Rh6G-(+)PBS-3′DABCYL allowed the formation of the extended (+)/(−)PBS duplex, causing an important increase of the dye-to-dye distance as evidenced by the Rh6G fluorescence restoration. In the absence of peptide, the (+)/(−)PBS hybridization spontaneously occurred with a rather slow rate (Table 3). In the presence of NCp7, an about two orders of magnitude increase in the rate of the (+)/(−)PBS annealing reaction was observed. The NC(11–55) and $L_{37}$NC(11–55) mutants also increased the annealing reaction rate, albeit to a lesser extent than NCp7 (5- to 6-fold increase). Interestingly, a much stronger increase (30-fold) in the annealing rate was obtained with the $(SSHS)_2$NC(11–55) mutant (see Supplementary Figure S1 of the Supplementary Data). Since this mutant was shown to primarily promote annealing reactions through its electrostatic nucleic acid aggregating component (43,44), it is likely that this basic component plays a major role in the (+)/(−)PBS annealing rate.

To further dissect the effect of the NCp7 mutants on the (+)/(−)PBS annealing reaction, we monitored the annealing reaction in the temperature range of 5–50°C and plotted the reaction rates through an Arrhenius plot (Figure 4). According to the Arrhenius model, the transition state thermodynamic parameters can be derived from the reaction rates using:

$$k = A \times \exp\left(\frac{-E_a}{RT}\right) \quad (4)$$

where $A$ is a pre-exponential factor, $E_a$ is the activation energy, $R$ the gas constant and $T$ the temperature. In line with the Arrhenius model, the logarithm of the bimolecular rate constants was linearly dependent on the inverse of the temperature. Interestingly, the fits of the experimental data in the absence or the presence of the different NC mutants resulted in parallel lines (Figure 4), indicating that the activation energies ($E_a$) needed for the reaction to be productive (and their related ΔH* values) were poorly influenced by NCp7 and its mutants (Table 4). In sharp contrast, the annealing rates ($k$) were strongly dependent on the presence and nature of the NC peptide, giving significant variation of the Gibbs free energy $\Delta G^*$, according to:

$$\Delta G^* = -RT \ln\left(\frac{k.h}{k_B.T}\right) \quad (5)$$

where $h$ and $k_B$ are the Planck and Boltzmann constants, respectively. As the $\Delta H^*$ value was invariant for all NCp7 derivatives, changes in $\Delta G^*$ resulted from changes in the activation entropy of the reaction ($\Delta S^*$) (Table 3). The highest $\Delta S^*$ values were observed with the native NCp7 and the $(SSHS)_2$NC(11–55), while a much lower value was observed for the NC(11–55) mutant. The high $\Delta S^*$ values observed with NCp7 and $(SSHS)_2$NC(11–55) are possibly related to the high rates at which collisions occur between the ODNs coated by these peptides. The basic $N_{terminal}$

**Table 3.** Kinetic parameters of the annealing of (+)PBS to (−)PBS mutants in the absence and in the presence of NC derivatives

| Labelled sequence | Complementary sequence | $k$ ($M^{-1}$ $s^{-1}$) | | | | |
|---|---|---|---|---|---|---|
| | | – | NCp7 | NC(11–55) | $L_{37}$NC(11–55) | $(SSHS)_2$NC(11–55) |
| (+)PBS | (−)PBS | 3800[a] ± 100 | 180 000[a] ± 10 000 | 18 400[a] ± 1200 | 22 600 ± 2000 | 99 000 ± 6500 |
| | $A_5$(−)PBS | 3200[a] ± 100 | –[b] | –[b] | 18 000 ± 3000 | 64 000 ± 4000 |
| | $T_4$(−) PBS | ~20[a] | 210 000 ± 20 000 | 11 100[a] ± 200 | 6000 ± 1000 | 7000 ± 500 |

[a]Data from Ramalanjaona *et al*. (10).
[b]No rate constant could be defined since NCp7 promotes the dissociation of the A5(−)/(+)PBS duplex.

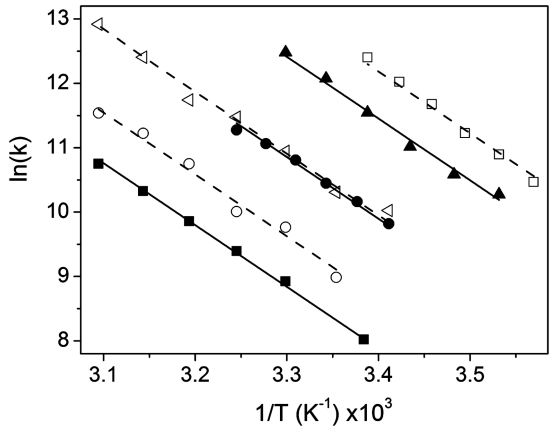


**Figure 4.** Arrhenius analysis of the annealing of (−)PBS to (+)PBS in the presence of NCp7 mutants. The experiments were performed in the absence (closed squares) or in the presence of NCp7 (open squares) or its mutants, NC(11–55) (closed circles), $SSHS_2$NC(11–55) (closed triangles), $A_{16}$NC(11–55) (open circles) and $L_{37}$NC(11–55) (open triangles).

domain of NCp7 and the unfolded $(SSHS)_2$NC(11–55) peptide probably efficiently screen the negatively charged ODNs and create short range interactions between the complementary ODNs, even at sub-aggregating concentrations (5). This 'aggregation' or molecular crowding effect is thought to facilitate the diffusional search for the complementary sequences (45) and increase the reaction rate.

Next, we performed a (−)PBS mutational analysis to determine the reaction pathways in the presence of NCp7 and NC mutants. The annealing experiments were first performed with the $A_5$(−)PBS mutant (Figure 5A) which prevents the annealing pathway initiated through the loops (Figure 5A). With both NCp7 and NC(11–55), no accumulation of extended duplexes was observed, due to the ability of both peptides to dissociate the duplexes of (+)PBS with $A_5$(−)PBS that spontaneously form in the absence of peptide (10). In sharp contrast, both $L_{37}$NC(11–55) and $(SSHS)_2$NC(11–55) strongly promoted the annealing of (+)PBS to $A_5$(−)PBS, with annealing rates close to those observed with the native (+)/(−)PBS sequences, suggesting that the (−)PBS loop does not play a critical role in the reaction pathway promoted by these NC mutants (Table 3).

We also investigated the annealing reaction of (+)PBS with a $T_4$(−)PBS mutant, in which the 15-GCCA-18 sequence was substituted by a $T_4$ sequence to prevent the nucleation through the PBS single strand overhangs (Figure 5B). In the presence of NCp7 or NC(11–55), the rate constants with the $T_4$(−)PBS mutant were similar to those with the native (−)PBS, suggesting that the (−)PBS overhang is not critical for the main reaction pathway promoted by NCp7 and NC(11–55). In contrast, a 15- and 4-fold decrease in the annealing rates were observed when the corresponding annealing reactions were monitored with $(SSHS)_2$NC(11–55) or $L_{37}$NC(11–55), respectively (Table 3). This clearly indicated that the (−)PBS overhang plays a central role in the $(SSHS)_2$NC(11–55)-promoted (+)/(−)PBS annealing reaction, and to a lesser extent in the $L_{37}$NC(11–55)-promoted (+)/(−)PBS annealing reaction.

Thus, our data strongly suggest that $(SSHS)_2$NC(11–55) or $L_{37}$NC(11–55) promote the (+)/(−)PBS annealing reaction, mainly through the single-strand overhangs at the bottom of the PBS stems, while, NCp7 and NC(11–55) promote this reaction mainly through the loops. Thus, the activity of NCp7 mutants on the loop dynamics correlates well with their ability to promote the (+)/(−)PBS annealing reaction through the loops. Therefore, the NCp7-induced restriction of the local and overall dynamics of the PBS loop likely constitutes a molecular prerequisite for promoting the (+)/(−)PBS annealing reaction through the loop–loop kissing pathway.

## DISCUSSION

In this study, we investigated the mechanism of NCp7-directed (+)/(−)PBS annealing that occurs during the plus DNA strand transfer reaction. To this end, we used ΔP(−)PBS and ΔP(+)PBS stem–loops substituted with 2-Ap to characterize the structural and dynamical changes in the loop induced by NCp7 or NC mutants, and to correlate these changes with the thermodynamic and kinetic parameters of the annealing reaction.

The substitution of natural bases by 2-Ap in the PBS loops was shown to minimally affect the folding of the loop and its binding parameters to NCp7. In the absence of protein, the 2-Ap residues in both (−)PBS and (+)PBS loops experienced multiple conformations and were efficiently quenched through collisions with their neighbour residues, in line with an orientation of the bases toward the interior of the loop and a partial order of the loop (13,34). NCp7 restricted the picosecond to nanosecond dynamics of the PBS loops, by

**Table 4.** Thermodynamic parameters of the NC-promoted (+)/(−)PBS annealing

| | $k^a$ ($M^{-1}$ $s^{-1}$) | $E_a{}^b$ (kJ/mol) | $\Delta G^{*c}$ (kJ/mol) | $\Delta H^{*d}$ (kJ/mol) | $\Delta S^{*e}$ (*eu*) |
|---|---|---|---|---|---|
| No peptide | $4.3 \pm 1.0 \times 10^3$ | 80 ± 8 | 57 | 78 ± 5 | 17 ± 3 |
| NCp7 | $3.2 \pm 1.0 \times 10^5$ | 78 ± 10 | 45 | 76 ± 8 | 26 ± 3 |
| NC(11–55) | $3.1 \pm 0.6 \times 10^4$ | 78 ± 12 | 52 | 76 ± 9 | 19 ± 2 |
| $A_{16}$NC(11–55) | $9.4 \pm 0.7 \times 10^3$ | 80 ± 8 | 55 | 78 ± 6 | 17 ± 2 |
| $L_{37}$ NC(11–55) | $3.2 \pm 0.8 \times 10^4$ | 77 ± 11 | 48 | 74 ± 8 | 18 ± 2 |
| $SSHS_2$ NC(11–55) | $1.8 \pm 0.6 \times 10^5$ | 81 ± 9 | 48 | 79 ± 7 | 25 ± 3 |

[a]Determined at 25°C.
[b]Determined from the Arrhenius plot (Figure 4).
[c]Calculated from the annealing rate constant at 25°C according to Equation (5).
[d]$\Delta$H* is given by $\Delta H^* = E_a - RT$ with $T = 298.15$ K.
[e]Calculated according to $\Delta G^* = \Delta H^* - T\Delta S^*$. *eu* corresponds to (cal $mol^{-1}$ $K^{-1}$)

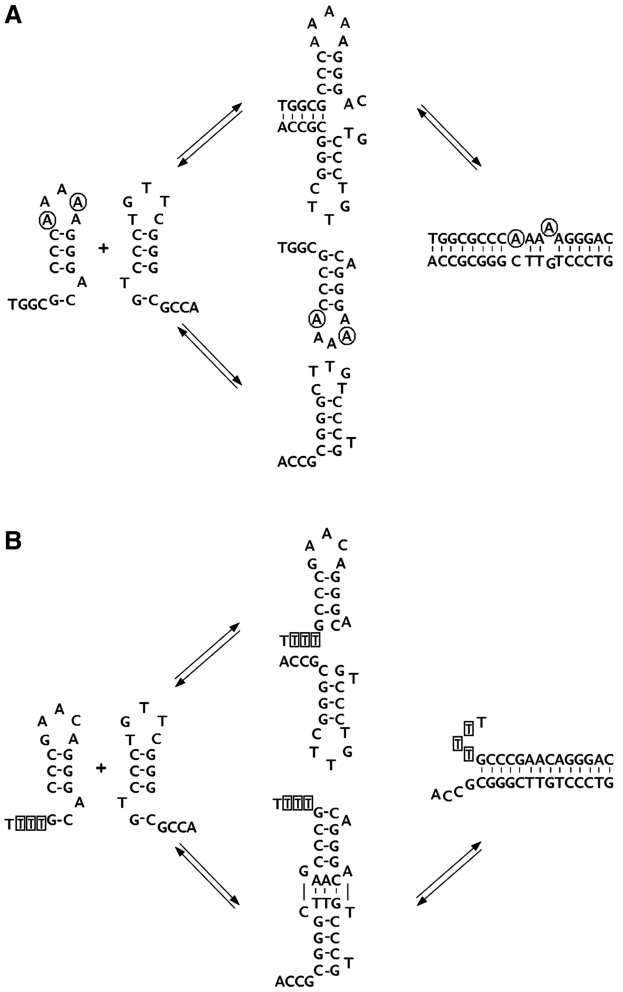


**Figure 5.** (−)PBS mutational analysis of the annealing reaction. (**A**) The $A_5$(−)PBS derivative (mutated residues are surrounded by a circle) was designed to prevent loop–loop interactions. No $A_5$(−)PBS/(+)PBS duplex accumulated in the presence of NCp7. In contrast, NC ZF mutants strongly promoted the $A_5$(−)PBS/(+)PBS annealing reaction. (**B**) The $T_4$(−)PBS derivative (mutated residues are surrounded by a rectangle) was designed to prevent the nucleation of the two complementary PBS sequence through the ss overhangs. Annealing of $T_4$(−)PBS with (+)PBS occurred at low rate in the absence of NCp7 or in the presence of NCp7 mutants with altered chaperone properties. In contrast, in the presence of NCp7, the $T_4$(−)PBS/(+)PBS annealing reaction occurred at a rate similar to that observed with the native DNA sequences.

constraining both the overall flexibility of the loops and the local mobility of the bases. Similar effects of NCp7 were previously observed with small flexible single-stranded ODNs (26,27), suggesting that they correspond to a general feature of interaction between NCp7 and its binding sites. The observed changes in the loop dynamics of both (+)PBS and (−)PBS species and the resulting base unstacking clearly suggested that NCp7 stabilizes conformations where the loop is stretched. Using NC mutants, the dynamic changes in the PBS loops were found to result from the specific interaction with the hydrophobic plateau at the top of the folded ZFs that also supports the destabilizing component of the NCp7 chaperone activity. Most interestingly, the NCp7-induced restriction of the dynamics in the PBS loops strongly correlated with the ability of NCp7 to switch the (−)/(+) PBS annealing reaction from a single strand overhangs pathway (Figure 6, upper pathway) to a loop–loop kissing pathway (Figure 6, lower pathway). Mutating the critical $F_{16}$ and $W_{37}$ aromatic amino acids in the two ZFs resulted in a very limited restriction of the loop mobility. Since these NC mutants only promoted slightly the switching of annealing pathway, one can speculate that the dynamics of the whole PBS loop should be restricted to induce this switching. As the PBS loop can accommodate two NCp7 protein molecules (13), an appropriate restriction of the loop dynamics probably requires the binding of two native NC molecules.

From the temperature dependence of the annealing rate, it appears that NCp7 does not lower the activation energy $E_a$ of the annealing reaction. In fact, the corresponding positive enthalpy ($\Delta H^* \sim 77$ kJ/mol) (Table 4) is consistent with the melting of about 3–4 base pairs (43,46), indicating that the melting of the PBS stem probably constitutes the rate-limiting step of the annealing reaction (10). Since the $E_a$ value was not affected by NCp7 or its mutants, the transition state of the reaction probably remains the same in all pathways and thus constitutes a saddle point in the energy landscape. Furthermore, the absence of NCp7-induced changes in the $\Delta H^*$ value was fully consistent with the previously reported inability of NCp7 to melt the stable (−)PBS stem (8,9).

Comparison of the annealing rates of NCp7 and NC(11–55) confirmed that the N-terminal domain of

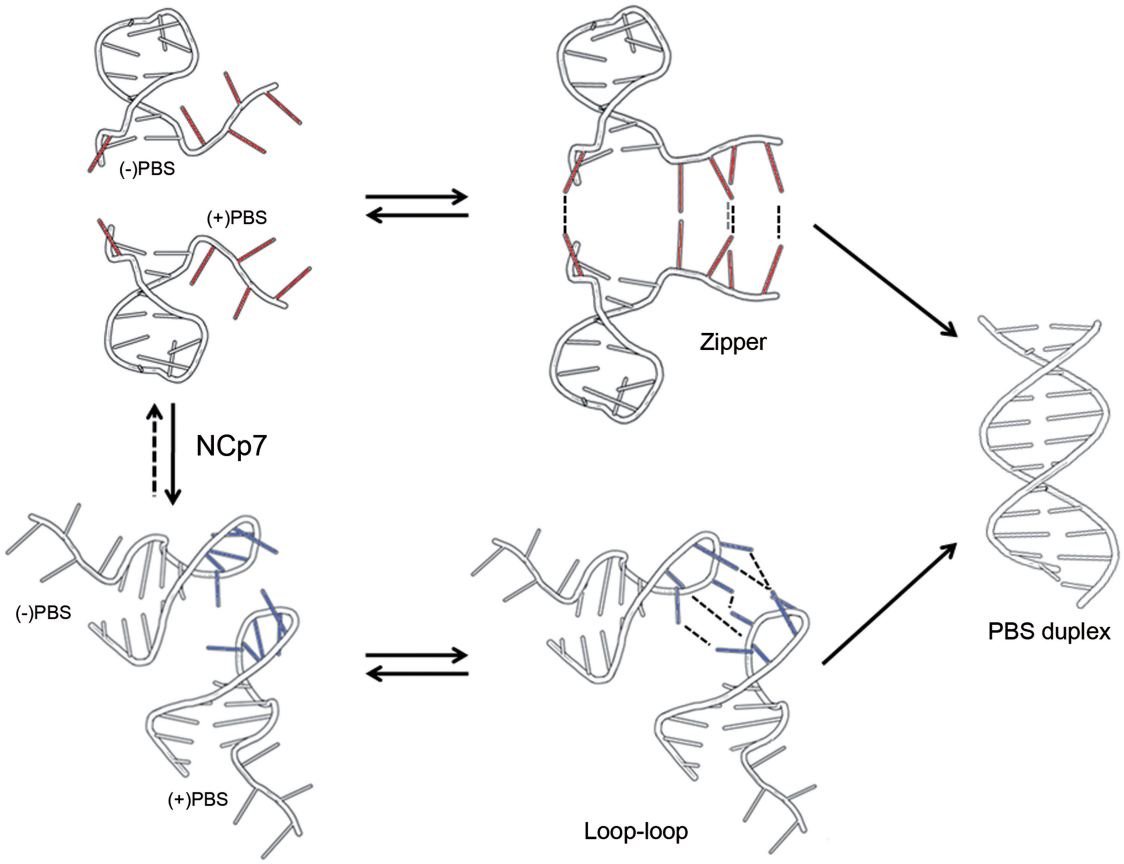


**Figure 6.** Proposed mechanism for (−)/(+)PBS annealing. In the absence of NCp7 (upper pathway), the bases of (−)PBS and (+)PBS loops are oriented towards the interior of the loop and not available for loop–loop interaction. As a consequence, the annealing is nucleated through the flexible single-stranded overhangs and possibly, the exposed bulged nt at the bottom of the stem (red bases). In contrast, upon the preferential binding to the PBS loops, NCp7 stretches the loop and exposes the loop bases (blue bases, lower pathway). As a result, NCp7 'freezes' PBS conformations competent for annealing via the loops, leading to a strong activation of the loop–loop kissing pathway, and thus, to a switch in the reaction mechanism.

NCp7 plays a central role in determining the annealing reaction rates. Since this domain largely governs the aggregating properties of the protein (44,47,48), the resulting crowding effect is probably responsible for the high $\Delta S^*$ value in the presence of NCp7. The $\Delta S^*$ value and the annealing rate were also high in the presence of $(SSHS)_2NC(11–55)$. The flexible nature of this mutant may allow it to better adjust to the ODN structure and thus, better screen the repulsive forces between the ODN phosphate charges, which results in a more efficient promotion of the annealing reaction. A similar improved performance of a SSHS(1–55) mutant as compared to the native NCp7 was previously reported for the annealing of $tRNA^{Lys3}$ to the PBS sequence (43). In addition, since this mutant does not destabilize the ODN structure, the enhancement in annealing rate appears thus poorly related to the destabilizing activity of NCp7.

In sharp contrast, the ability of the mutants to induce a mechanistic switch strongly depends on the integrity of the hydrophobic platform on the ZF domain. Mutations preventing the formation of this platform and thus, abolishing the nucleic acid destabilizing activity of NCp7 (40,44,49) were unable to induce this mechanistic switch, but can still accelerate the annealing reaction. In this context, the chaperoning activity of NCp7 can be appropriately envisioned only if the annealing pathway is considered. The disregard of the annealing pathway probably explains previous *in vitro* observations where the ZFs of NCp7 were reported to be dispensable in promoting annealing reactions (50–52). In sharp contrast to these *in vitro* experiments, even single point mutations within the ZFs resulted in the production of non-infectious particles *in vivo*, clearly showing that the ZFs play a critical role (53–56). Mutations in the NCp7 ZFs resulted notably in lower plus strand transfer efficiency, defective viral DNA (vDNA) sequences, and profound modifications of the spatio-temporal control of the reverse transcription process (56–63). Nevertheless, in line with our observations that ZF mutations still allow efficient (−)/(+)PBS annealing, the corresponding mutants do not block *in vivo* the synthesis of viral DNA (62–64). This is likely related to the ability of the mutated NC proteins to stimulate non-specifically the rearrangements of nucleic acids through pathways already existing in the absence of peptides (i.e. mostly through the PBS overhangs here). Such a non-specific promotion may also exist in various

physiological microenvironments rich in polycations, such as the seminal fluid, that promote the natural endogenous reverse transcription (65,66). In contrast, the binding of wild-type NCp7 to both (−)PBS and (+)PBS loops reveals hidden nucleation sites which fuels nucleic acid rearrangements towards specific routes. Both the switch in the annealing mechanism and the inhibition of the annealing of imperfect complementary sequences [see mutant $A_5$(−)PBS in Table 3] constitute two clear examples of how NCp7 directs the nucleic acid rearrangements towards such specific routes. Interestingly, NCp7 also induces a switch of the annealing pathway during the first strand transfer by directing the hybridization of the TAR complementary sequences via the ends of their double-stranded stems (45,67). These two switches, from the loop to the stem for TAR/cTAR and from the overhangs to the loop for (+)/(−)PBS, are clearly related to the ability of NCp7 to locally destabilize these sequences. Indeed, NCp7 destabilizes mainly the bottom of the cTAR stem and poorly the top of the stem–loop (21,68–72) while it mainly affects the loop of the PBS sequences (9,13). Thus, the ability of NCp7 to funnel nucleic acid rearrangements towards specific routes appears to be strongly dependent on the sequence/structure context and is probably of importance for the control of reverse transcription timing and ultimately for the generation of stable vDNA products.

NCp7 with properly folded ZFs was reported to improve the fidelity of reverse transcription by strongly inhibiting non-PPT priming, ensuring the selection of the PPT sequence as the sole primer for initiation of plus-strand DNA synthesis (73,74). In this respect, the ability of NCp7 to promote a specific annealing pathway during the second strand transfer could constitute a supplementary assertion in the understanding of how NCp7 ensures the formation of stable vDNA products. At the molecular level, both the plus priming control and the annealing mechanism selection require the hydrophobic platform at the top of the folded ZFs. Since this hydrophobic plateau is also the protein determinant associated with the destabilizing activity of NCp7, it could be of interest to determine whether NCp7 can also 'freeze' specific reactive states involved in the first strand transfer (67,75,76). This work is under progress.

## SUPPLEMENTARY DATA

Supplementary Data are available at NAR Online.

## ACKNOWLEDGEMENT

We acknowledge Etienne Piémont for his help in performing time-resolved experiments.

## FUNDING

Funding for open access charge: Agence Nationale de Recherches sur le SIDA.

*Conflict of interest statement*. None declared.

## REFERENCES

1. Basu,V.P., Song,M., Gao,L., Rigby,S.T., Hanson,M.N. and Bambara,R.A. (2008) Strand transfer events during HIV-1 reverse transcription. *Virus Res.*, **134**, 19–38.
2. Darlix,J.L., Lapadat-Tapolsky,M., de Rocquigny,H. and Roques,B.P. (1995) First glimpses at structure–function relationships of the nucleocapsid protein of retroviruses. *J. Mol. Biol.*, **254**, 523–537.
3. Cristofari,G. and Darlix,J.L. (2002) The ubiquitous nature of RNA chaperone proteins. *Prog. Nucleic Acid Res. Mol. Biol.*, **72**, 223–268.
4. Darlix,J.L., Cristofari,G., Rau,M., Péchoux,C., Berthoux,L. and Roques,B. (2000) Nucleocapsid protein of human immunodeficiency virus as a model protein with chaperoning functions and as a target for antiviral drugs. *Adv. Pharmacol.*, **48**, 345–372.
5. Levin,J.G., Guo,J., Rouzina,I. and Musier-Forsyth,K. (2005) Nucleic acid chaperone activity of HIV-1 nucleocapsid protein: critical role in reverse transcription and molecular mechanism. *Prog. Nucleic Acid Res. Mol. Biol.*, **80**, 217–286.
6. Rein,A., Henderson,L.E. and Levin,J.G. (1998) Nucleic-acid-chaperone activity of retroviral nucleocapsid proteins: significance for viral replication. *Trends Biochem. Sci.*, **23**, 297–301.
7. Mély,Y., Rocquigny,H.D., Morellet,N., Roques,B.P. and Gérad,D. (1996) Zinc binding to the HIV-1 nucleocapsid protein: a thermodynamic investigation by fluorescence spectroscopy. *Biochemistry*, **35**, 5175–5182.
8. Egelé,C., Schaub,E., Piémont,E., de Rocquigny,H. and Mély,Y. (2005) Investigation by fluorescence correlation spectroscopy of the chaperoning interactions of HIV-1 nucleocapsid protein with the viral DNA initiation sequences. *C R Biol.*, **328**, 1041–1051.
9. Egelé,C., Schaub,E., Ramalanjaona,N., Piémont,E., Ficheux,D., Roques,B., Darlix,J.-L. and Mély,Y. (2004) HIV-1 nucleocapsid protein binds to the viral DNA initiation sequences and chaperones their kissing interactions. *J. Mol. Biol.*, **342**, 453–466.
10. Ramalanjaona,N., de Rocquigny,H., Millet,A., Ficheux,D., Darlix,J.-L. and Mély,Y. (2007) Investigating the mechanism of the nucleocapsid protein chaperoning of the second strand transfer during HIV-1 DNA synthesis. *J. Mol. Biol.*, **374**, 1041–1053.
11. Wu,T., Guo,J., Bess,J., Henderson,L.E. and Levin,J.G. (1999) Molecular requirements for human immunodeficiency virus type 1 plus-strand transfer: analysis in reconstituted and endogenous reverse transcription systems. *J. virol.*, **73**, 4794–4805.
12. Herschlag,D. (1995) RNA chaperones and the RNA folding problem. *J. Biol. Chem.*, **270**, 20871–20874.
13. Bourbigot,S., Ramalanjaona,N., Boudier,C., Salgado,G.F.J., Roques,B.P., Mély,Y., Bouaziz,S. and Morellet,N. (2008) How the HIV-1 nucleocapsid protein binds and destabilises the (–)primer binding site during reverse transcription. *J. Mol. Biol.*, **383**, 1112–1128.
14. Lee,B.M., Guzman,R.N.D., Turner,B.G., Tjandra,N. and Summers,M.F. (1998) Dynamical behavior of the HIV-1 nucleocapsid protein. *J. Mol. Biol.*, **279**, 633–649.
15. Mély,Y., Jullian,N., Morellet,N., Rocquigny,H.D., Dong,C.Z., Piémont,E., Roques,B.P. and Gérard,D. (1994) Spatial proximity of the HIV-1 nucleocapsid protein zinc fingers investigated by time-resolved fluorescence and fluorescence resonance energy transfer. *Biochemistry*, **33**, 12085–12091.
16. Morellet,N., de Rocquigny,H., Mély,Y., Jullian,N., Déméné,H., Ottmann,M., Gérard,D., Darlix,J.L., Fournie-Zaluski,M.C. and Roques,B.P. (1994) Conformational behaviour of the active and inactive forms of the nucleocapsid NCp7 of HIV-1 studied by 1H NMR. *J. Mol. Biol.*, **235**, 287–301.
17. Mori,M., Dietrich,U., Manetti,F. and Botta,M. (2010) Molecular dynamics and DFT study on HIV-1 nucleocapsid protein-7 in complex with viral genome. *J. Chem. Inf. Model*, **50**, 638–650.
18. Ward,D.C., Reich,E. and Stryer,L. (1969) Fluorescence studies of nucleotides and polynucleotides. I. Formycin, 2-aminopurine riboside, 2,6-diaminopurine riboside, and their derivatives. *J. Biol. Chem.*, **244**, 1228–1237.

19. de Rocquigny,H., Ficheux,D., Gabus,C., Fournie-Zaluski,M.C., Darlix,J.L. and Roques,B.P. (1991) First large scale chemical synthesis of the 72 amino acid HIV-1 nucleocapsid protein NCp7 in an active form. *Biochem. Biophys. Res. Commun.*, **180**, 1010–1018.
20. Shvadchak,V.V., Klymchenko,A.S., de Rocquigny,H. and Mély,Y. (2009) Sensing peptide-oligonucleotide interactions by a two-color fluorescence label: application to the HIV-1 nucleocapsid protein. *Nucleic Acids Res.*, **37**, e25.
21. Bernacchi,S., Stoylov,S., Piémont,E., Ficheux,D., Roques,B.P., Darlix,J.L. and Mély,Y. (2002) HIV-1 nucleocapsid protein activates transient melting of least stable parts of the secondary structure of TAR and its complementary sequence. *J. Mol. Biol.*, **317**, 385–399.
22. Brochon,J.C. (1994) Maximum entropy method of data analysis in time-resolved spectroscopy. *Methods Enzymol.*, **240**, 262–311.
23. Livesey,A.K. and Brochon,J.C. (1987) Analyzing the distribution of decay constants in pulse-fluorimetry using the maximum entropy method. *Biophys. J.*, **52**, 693–706.
24. Jean,J.M. and Hall,K.B. (2001) 2-Aminopurine fluorescence quenching and lifetimes: role of base stacking. *Proc. Natl Acad. Sci. USA*, **98**, 37–41.
25. Guest,C.R., Hochstrasser,R.A., Sowers,L.C. and Millar,D.P. (1991) Dynamics of mismatched base pairs in DNA. *Biochemistry*, **30**, 3271–3279.
26. Avilov,S., Godet,J., Piemont,E. and Mély,Y. (2009) Site-specific characterization of HIV-1 nucleocapsid protein binding to oligonucleotides with two binding sites. *Biochemistry*, **48**, 2422–2430.
27. Avilov,S.V., Piemont,E., Shvadchak,V., de Rocquigny,H. and Mély,Y. (2008) Probing dynamics of HIV-1 nucleocapsid protein/target hexanucleotide complexes by 2-aminopurine. *Nucleic Acids Res.*, **36**, 885–896.
28. Jean,J.M. and Hall,K.B. (2002) 2-Aminopurine electronic structure and fluorescence properties in DNA. *Biochemistry*, **41**, 13152–13161.
29. Larsen,O.F., van Stokkum,I.H., Gobets,B., van Grondelle,R. and van Amerongen,H. (2001) Probing the structure and dynamics of a DNA hairpin by ultrafast quenching and fluorescence depolarization. *Biophys. J.*, **81**, 1115–1126.
30. Wan,C., Fiebig,T., Schiemann,O., Barton,J.K. and Zewail,A.H. (2000) Femtosecond direct observation of charge transfer between bases in DNA. *Proc. Natl Acad. Sci. USA*, **97**, 14052–14055.
31. Fiebig,T., Wan,C. and Zewail,A.H. (2002) Femtosecond charge transfer dynamics of a modified DNA base: 2-aminopurine in complexes with nucleotides. *Chemphyschem*, **3**, 781–788.
32. O'Neill,M.A. and Barton,J.K. (2002) 2-Aminopurine: a probe of structural dynamics and charge transfer in DNA and DNA:RNA hybrids. *J. Am. Chem. Soc.*, **124**, 13053–13066.
33. Jean,J.M. and Hall,K.B. (2004) Stacking–unstacking dynamics of oligodeoxynucleotide trimers. *Biochemistry*, **43**, 10277–10284.
34. Johnson,P.E., Turner,R.B., Wu,Z.R., Hairston,L., Guo,J., Levin,J.G. and Summers,M.F. (2000) A mechanism for plus-strand transfer enhancement by the HIV-1 nucleocapsid protein during reverse transcription. *Biochemistry*, **39**, 9084–9091.
35. Lakowicz,J.R. (1999) *Principles of Fluorescence Spectroscopy*, 2nd edn. Kluwer Academic/Plenum Publishers, New York.
36. Mely,Y., de Rocquigny,H., Piémont,E., Déméné,H., Jullian,N., Fournié-Zaluski,M.C., Roques,B. and Gérard,D. (1993) Influence of the N- and C-terminal chains on the zinc-binding and conformational properties of the central zinc-finger structure of Moloney murine leukaemia virus nucleocapsid protein: a steady-state and time-resolved fluorescence study. *Biochim. Biophys. Acta*, **1161**, 6–18.
37. Vuilleumier,C., Bombarda,E., Morellet,N., Gérard,D., Roques,B.P. and Mély,Y. (1999) Nucleic acid sequence discrimination by the HIV-1 nucleocapsid protein NCp7: a fluorescence study. *Biochemistry*, **38**, 16816–16825.
38. Green,L.M. and Berg,J.M. (1990) Retroviral nucleocapsid protein–metal ion interactions: folding and sequence variants. *Proc. Natl Acad. Sci. USA*, **87**, 6403–6407.
39. Guo,J., Wu,T., Anderson,J., Kane,B.F., Johnson,D.G., Gorelick,R.J., Henderson,L.E. and Levin,J.G. (2000) Zinc finger structures in the human immunodeficiency virus type 1 nucleocapsid protein facilitate efficient minus- and plus-strand transfer. *J. Virol.*, **74**, 8980–8988.
40. Beltz,H., Clauss,C., Piémont,E., Ficheux,D., Gorelick,R.J., Roques,B., Gabus,C., Darlix,J.-L., de Rocquigny,H. and Mély,Y. (2005) Structural determinants of HIV-1 nucleocapsid protein for cTAR DNA binding and destabilization, and correlation with inhibition of self-primed DNA synthesis. *J. Mol. Biol.*, **348**, 1113–1126.
41. Fisher,R.J., Fivash,M.J., Stephen,A.G., Hagan,N.A., Shenoy,S.R., Medaglia,M.V., Smith,L.R., Worthy,K.M., Simpson,J.T., Shoemaker,R. *et al.* (2006) Complex interactions of HIV-1 nucleocapsid protein with oligonucleotides. *Nucleic Acids Res.*, **34**, 472–484.
42. Gorelick,R.J., Gagliardi,T.D., Bosche,W.J., Wiltrout,T.A., Coren,L.V., Chabot,D.J., Lifson,J.D., Henderson,L.E. and Arthur,L.O. (1999) Strict conservation of the retroviral nucleocapsid protein zinc finger is strongly influenced by its role in viral infection processes: characterization of HIV-1 particles containing mutant nucleocapsid zinc-coordinating sequences. *Virology*, **256**, 92–104.
43. Hargittai,M.R.S., Gorelick,R.J., Rouzina,I. and Musier-Forsyth,K. (2004) Mechanistic insights into the kinetics of HIV-1 nucleocapsid protein-facilitated tRNA annealing to the primer binding site. *J. Mol. Biol.*, **337**, 951–968.
44. Williams,M.C., Rouzina,I., Wenner,J.R., Gorelick,R.J., Musier-Forsyth,K. and Bloomfield,V.A. (2001) Mechanism for nucleic acid chaperone activity of HIV-1 nucleocapsid protein revealed by single molecule stretching. *Proc. Natl Acad. Sci. USA*, **98**, 6121–6126.
45. Vo,M.-N., Barany,G., Rouzina,I. and Musier-Forsyth,K. (2009) HIV-1 nucleocapsid protein switches the pathway of transactivation response element RNA/DNA annealing from loop–loop "kissing" to "zipper". *J. Mol. Biol.*, **386**, 789–801.
46. Rouzina,I. and Bloomfield,V.A. (1999) Heat capacity effects on the melting of DNA. 1. General aspects. *Biophys. J.*, **77**, 3242–3251.
47. Le Cam,E., Coulaud,D., Delain,E., Petitjean,P., Roques,B.P., Gerard,D., Stoylova,E., Vuilleumier,C., Stoylov,S.P. and Mely,Y. (1998) Properties and growth mechanism of the ordered aggregation of a model RNA by the HIV-1 nucleocapsid protein: an electron microscopy investigation. *Biopolymers*, **45**, 217–229.
48. Stoylov,S.P., Vuilleumier,C., Stoylova,E., De Rocquigny,H., Roques,B.P., Gerard,D. and Mely,Y. (1997) Ordered aggregation of ribonucleic acids by the human immunodeficiency virus type 1 nucleocapsid protein. *Biopolymers*, **41**, 301–312.
49. Williams,M.C., Gorelick,R.J. and Musier-Forsyth,K. (2002) Specific zinc-finger architecture required for HIV-1 nucleocapsid protein's nucleic acid chaperone function. *Proc. Natl Acad. Sci. USA*, **99**, 8614–8619.
50. De Rocquigny,H., Gabus,C., Vincent,A., Fournie-Zaluski,M.C., Roques,B. and Darlix,J.L. (1992) Viral RNA annealing activities of human immunodeficiency virus type 1 nucleocapsid protein require only peptide domains outside the zinc fingers. *Proc. Natl Acad. Sci. USA*, **89**, 6472–6476.
51. Lapadat-Tapolsky,M., Gabus,C., Rau,M. and Darlix,J.L. (1997) Possible roles of HIV-1 nucleocapsid protein in the specificity of proviral DNA synthesis and in its variability. *J. Mol. Biol.*, **268**, 250–260.
52. Prats,A.C., Housset,V., de Billy,G., Cornille,F., Prats,H., Roques,B. and Darlix,J.L. (1991) Viral RNA annealing activities of the nucleocapsid protein of Moloney murine leukemia virus are zinc independent. *Nucleic Acids Res.*, **19**, 3533–3541.
53. Dorfman,T., Luban,J., Goff,S.P., Haseltine,W.A. and Gottlinger,H.G. (1993) Mapping of functionally important residues of a cysteine-histidine box in the human immunodeficiency virus type 1 nucleocapsid protein. *J. Virol.*, **67**, 6159–6169.
54. Gorelick,R.J., Benveniste,R.E., Gagliardi,T.D., Wiltrout,T.A., Busch,L.K., Bosche,W.J., Coren,L.V., Lifson,J.D., Bradley,P.J., Henderson,L.E. *et al.* (1999) Nucleocapsid protein zinc-finger mutants of simian immunodeficiency virus strain mne produce virions that are replication defective *in vitro* and *in vivo*. *Virology*, **253**, 259–270.

55. Gorelick,R.J., Chabot,D.J., Rein,A., Henderson,L.E. and Arthur,L.O. (1993) The two zinc fingers in the human immunodeficiency virus type 1 nucleocapsid protein are not functionally equivalent. *J. Virol.*, **67**, 4027–4036.
56. Tanchou,V., Decimo,D., Péchoux,C., Lener,D., Rogemond,V., Berthoux,L., Ottmann,M. and Darlix,J.L. (1998) Role of the N-terminal zinc finger of human immunodeficiency virus type 1 nucleocapsid protein in virus structure and replication. *J. Virol.*, **72**, 4442–4447.
57. Buckman,J.S., Bosche,W.J. and Gorelick,R.J. (2003) Human immunodeficiency virus type 1 nucleocapsid zn(2+) fingers are required for efficient reverse transcription, initial integration processes, and protection of newly synthesized viral DNA. *J. Virol.*, **77**, 1469–1480.
58. Thomas,J.A. and Gorelick,R.J. (2008) Nucleocapsid protein function in early infection processes. *Virus Res.*, **134**, 39–63.
59. Didierlaurent,L., Houzet,L., Morichaud,Z., Darlix,J.-L. and Mougel,M. (2008) The conserved N-terminal basic residues and zinc-finger motifs of HIV-1 nucleocapsid restrict the viral cDNA synthesis during virus formation and maturation. *Nucleic Acids Res.*, **36**, 4745–4753.
60. Houzet,L., Morichaud,Z., Didierlaurent,L., Muriaux,D., Darlix,J.-L. and Mougel,M. (2008) Nucleocapsid mutations turn HIV-1 into a DNA-containing virus. *Nucleic Acids Res.*, **36**, 2311–2319.
61. Mougel,M., Houzet,L. and Darlix,J.-L. (2009) When is it time for reverse transcription to start and go? *Retrovirology*, **6**, 24.
62. Thomas,J.A., Gagliardi,T.D., Alvord,W.G., Lubomirski,M., Bosche,W.J. and Gorelick,R.J. (2006) Human immunodeficiency virus type 1 nucleocapsid zinc-finger mutations cause defects in reverse transcription and integration. *Virology*, **353**, 41–51.
63. Thomas,J.A., Shulenin,S., Coren,L.V., Bosche,W.J., Gagliardi,T.D., Gorelick,R.J. and Oroszlan,S. (2006) Characterization of human immunodeficiency virus type 1 (HIV-1) containing mutations in the nucleocapsid protein at a putative HIV-1 protease cleavage site. *Virology*, **354**, 261–270.
64. Coren,L.V., Thomas,J.A., Chertova,E., Sowder,R.C., Gagliardi,T.D., Gorelick,R.J. and Ott,D.E. (2007) Mutational analysis of the C-terminal gag cleavage sites in human immunodeficiency virus type 1. *J. Virol.*, **81**, 10047–10054.
65. Zhang,H., Dornadula,G. and Pomerantz,R.J. (1996) Endogenous reverse transcription of human immunodeficiency virus type 1 in physiological microenviroments: an important stage for viral infection of nondividing cells. *J. Virol.*, **70**, 2809–2824.
66. Zhang,H., Dornadula,G. and Pomerantz,R.J. (1998) Natural endogenous reverse transcription of HIV-1. *J. Reprod. Immunol*, **41**, 255–260.
67. Godet,J., de Rocquigny,H., Raja,C., Glasser,N., Ficheux,D., Darlix,J.-L. and Mély,Y. (2006) During the early phase of HIV-1 DNA synthesis, nucleocapsid protein directs hybridization of the TAR complementary sequences via the ends of their double-stranded stem. *J. Mol. Biol.*, **356**, 1180–1192.
68. Azoulay,J., Clamme,J.P., Darlix,J.L., Roques,B.P. and Mély,Y. (2003) Destabilization of the HIV-1 complementary sequence of TAR by the nucleocapsid protein through activation of conformational fluctuations. *J. Mol. Biol.*, **326**, 691–700.
69. Beltz,H., Azoulay,J., Bernacchi,S., Clamme,J.-P., Ficheux,D., Roques,B., Darlix,J.-L. and Mély,Y. (2003) Impact of the terminal bulges of HIV-1 cTAR DNA on its stability and the destabilizing activity of the nucleocapsid protein NCp7. *J. Mol. Biol.*, **328**, 95–108.
70. Beltz,H., Piémont,E., Schaub,E., Ficheux,D., Roques,B., Darlix,J.-L. and Mély,Y. (2004) Role of the structure of the top half of HIV-1 cTAR DNA on the nucleic acid destabilizing activity of the nucleocapsid protein NCp7. *J. Mol. Biol.*, **338**, 711–723.
71. Cosa,G., Harbron,E.J., Zeng,Y., Liu,H.-W., O'Connor,D.B., Eta-Hosokawa,C., Musier-Forsyth,K. and Barbara,P.F. (2004) Secondary structure and secondary structure dynamics of DNA hairpins complexed with HIV-1 NC protein. *Biophys. J.*, **87**, 2759–2767.
72. Cosa,G., Zeng,Y., Liu,H.-W., Landes,C.F., Makarov,D.E., Musier-Forsyth,K. and Barbara,P.F. (2006) Evidence for non-two-state kinetics in the nucleocapsid protein chaperoned opening of DNA hairpins. *J. Phys. Chem. B*, **110**, 2419–2426.
73. Jacob,D.T. and DeStefano,J.J. (2008) A new role for HIV nucleocapsid protein in modulating the specificity of plus strand priming. *Virology*, **378**, 385–396.
74. Post,K., Kankia,B., Gopalakrishnan,S., Yang,V., Cramer,E., Saladores,P., Gorelick,R.J., Guo,J., Musier-Forsyth,K. and Levin,J.G. (2009) Fidelity of plus-strand priming requires the nucleic acid chaperone activity of HIV-1 nucleocapsid protein. *Nucleic Acids Res.*, **37**, 1755–1766.
75. Liu,H.-W., Zeng,Y., Landes,C.F., Kim,Y.J., Zhu,Y., Ma,X., Vo,M.-N., Musier-Forsyth,K. and Barbara,P.F. (2007) Insights on the role of nucleic acid/protein interactions in chaperoned nucleic acid rearrangements of HIV-1 reverse transcription. *Proc. Natl Acad. Sci. USA*, **104**, 5261–5267.
76. Zeng,Y., Liu,H.-W., Landes,C.F., Kim,Y.J., Ma,X., Zhu,Y., Musier-Forsyth,K. and Barbara,P.F. (2007) Probing nucleation, reverse annealing, and chaperone function along the reaction path of HIV-1 single-strand transfer. *Proc. Natl Acad. Sci. USA*, **104**, 12651–12656.